Geoscience Letters

RESEARCH LETTER

Open Access

# Source mechanism of volcanic tectonic events from October 2010 to December 2011 at the Sinabung volcano area

Afnimar[1*], Ary Hidayat[1], Kristianto[2], Hetty Triastuty[2], Ahmad Basuki[2] and Novianti Indrastuti[2]

**Abstract**

From its first eruption at the end of August 2010, Mount Sinabung has been being seismically active. Thousands of micro earthquakes have occurred in the magma itself, in hydrothermal systems, and along nearby tectonic faults. The installation of a three-component seismometer network around the Sinabung volcano from October 2010 to December 2011 has encouraged more detailed study of the source characteristics of micro earthquakes. In this study, we conduct a focal mechanism analysis of volcanic tectonic (VT) activity during this period. This study delineates three kinds of faults around the volcano. First, a possible oblique-strike-slip fault that was "cut" by the volcano is confirmed. The fault parameters are a strike of 44.76°, a dip of 67.83° and a rake of 19.7°. Second, a normal-faulting zone associated with Kawar Lake is parametrized by a strike, dip and rake of 5.8°, 77.4°, and − 113.2°, respectively. Third, a clear hidden oblique strike-slip was found at the north-west part of the summit. The fault lineation is shown clearly by its hypocentre distribution and is parameterized by its strike of 213.15°, dip of 77.72°, and rake of − 20.04°.

**Keywords:** VT focal mechanism, Finding one hidden fault plane, Confirming two possible faults

## Introduction

The series of eruptions of the Sinabung volcano after a long period (~ 1200 years) of dormancy (Hendrasto et al. 2012; Prambada et al. 2010) occurred on 28th August, 29th August, 3rd September and 7th September 2010 (Iguchi et al. 2011; Hendrasto et al. 2012; Centre for Volcanology and Geologic Hazard Mitigation (CVGHM) internal report, 2013). All these eruptions were phreatic (Iguchi et al. 2011; Gunawan et al. 2019) and they had ceased by the end of September 2010. After that, Gunawan et al. (2019), McCausland et al. (2019) and Indrastuti et al. (2019) noticed a persistent state of low-level unrest indicated by the occurrence of only passive steam plumes and volcano-tectonic (VT) earthquakes. The VT earthquake is one type of event that occurs along a nearby tectonic fault caused by large-volume magma migration (e.g. Zobin 1972; Roman and Cashman, 2006; Zoback et al. 2013; Chouet and Matoza 2013; Dumont et al. 2015; McNutt and Roman 2015; White and McCausland 2016, 2019). In particular, White and McCausland 2016 found that this VT seismicity originates mostly on tectonic fault structures at distances of one or two to tens of kilometers laterally from the site of the eventual eruption and typically occurs as swarms rather than as mainshock-aftershock sequences.

Prambada et al. 2010 estimated the possible faults around the Sinabung area based on surface lineation. Figure 1b shows those faults that are generally possible strike-slip types. Only one fault located in the northern part of Kawar Lake is a normal fault type. The other possibilities are the existence of hidden faults covered by deposits. The distances between all these faults are less than ten kilometers and, according to the above explanations, the faults can be activated by magma migration. If

*Correspondence: afnimar.1987@gmail.com

[1] Seismology and Geodynamic Laboratory, Faculty of Mining and Petroleum Engineering, Bandung Institute of Technology (ITB), Ganesha 10 Street, West Java 40132, Bandung, Indonesia
Full list of author information is available at the end of the article

they are activated, the clusters of VT events will usually make lineations (e.g. White and McCausland 2019) from which the strikes and dips of fault planes can be estimated. The hypocentre distribution during this research period was located mostly at the northern part of the Sinabung summit (Indrastuti et al. 2019; Afnimar et al. 2020). There was one clear cluster with unclear lineation that was obtained from double-difference (DD) relocation (Afnimar et al. 2020). It was first thought that the clusters were related to magma migration. This hypothesis was corrected by Hotta et al. (2018) and Kriswati et al. (2018) who confirmed that no displacement evidence was related to magma intrusion in this area using GPS observation data, the cluster should be related to a fault plane.

Indrastuti et al. (2019) estimated the subsurface structure using the tomography method to collect travel time data, including the VT earthquake data used in this research. Unfortunately, the tomographic results did not resolve the fault structures around the Sinabung area. In this research, we study the source mechanisms of the VT events of the Sinabung volcano that are related to faults estimated by Prambada et al. (2010) and possible hidden faults. Finally, we interpret the local structure system in this area.

## Geological background

Mount Sinabung, a cone-type volcano, formed during the Pleistocene-Holocene era with andesitic and dacitic lava. This mountain is included in the Sunda volcanic arc formed from the subduction of the Indo-Australian plate under the Eurasian plate. The regional structure nearest to the Sinabung area is the Renum segment of the Sumatera fault zone (Sieh and Natawidjaja 2000) that elongate from the north-west to the south-east of Sumatera Island. Part of the Renum segment is placed along the western side of Toba Lake (Fig. 1a). The Sinabung area is located in the north-eastern parts, about 100 km from this segment. The possible local structure had been investigated by Prambada et al. (2010) (Fig. 1b). The Sinabung volcano is formed on the north-western edge of the fault of the old Toba basin. The possible sinistral-strike-slip fault line stretches from the western boundary of Toba to the north-eastern boundary. In the upper part of this fault, the Sinabung volcano formed in the south-west section and the Sibayak volcano formed in the northeast section. A normal fault structure is found in the Kawar Lake area (the northern part of the Sinabung summit in Fig. 1b). The hanging wall in the southern part is lower than its foot wall. This fault is characterized by triangular facet morphology, which is one of the characteristics of normal faults. This normal fault was formed by lossing of the pressure that caused decreasing the hanging wall block. In addition, other possible structures such as topographic straightness structures generally show a southwest-northeast orientation. The crater structure found at the top of the volcano also has a northwest-southeast orientation. The Sinabung volcano consists of 25 primary eruption rock units from the central crater

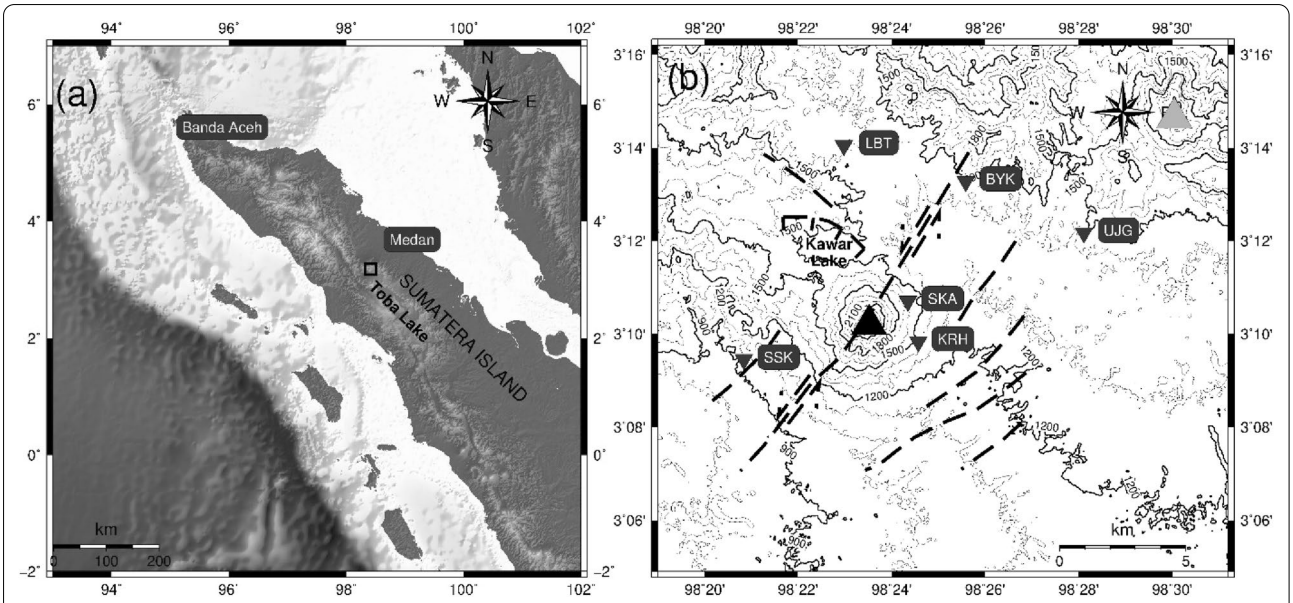


**Fig. 1** **a** The study area (black rectangle) is about 88 km from Medan, the capital city of North Sumatera Province. **b** The zoom of the black rectangle of (a). The black triangle is the summit of the Sinabung volcano and the grey one is the Sibayak volcano. The inverted triangles are seismic stations. The thick dashed lines are possible fault lines from Prambada et al. (2010)

and one section of secondary volcanic sediment. The Pre-Sinabung deposits in this area are in the form of limestone sediments and deposits of Toba pyroclastic flows. The youngest pyroclastic flow deposits date back to 1200 years ago, or 800—900 A.D. This young pyroclastic flow in the south-east part of the active crater is now the peak of Mount Sinabung.

## The data

The main data used in focal mechanism estimation are three-component seismogram data with 250 Hz sampling rate from the seismometer network (Fig. 1b) deployed by CVGHM from October 2010 to December 2011 to follow the phreatic eruptions in August and September 2010. During this period, swarms of proximal and distal VT earthquakes dominated (McCausland et al. 2019). The next data required concerns event locations. The event locations during that period had been investigated in detail by Afnimar et al. (2020). The best event locations were obtained by using the DD method (Waldhauser and Ellsworth 2000) with initial location from catalogue data obtained by Geiger's adaptive damping (GAD) method (Nishi 2005). The total number of 109 events that consist of 78 relocated and 31 un-relocated event locations is shown in Fig. 2. The data input of event locations were arrival times of direct P and S waves picked on waveforms generated by micro earthquakes using Seismic Analysis Code (SAC) from Goldstein and Snoke (2005). The events are distributed evenly, like the lineation found in the northern parts of the Sinabung summit. That particular cluster could relate to an activated fault, as we mentioned in the introduction. The next required data that include the geographic coordinates of each station are listed in Table 1. The 1D velocity model from Indrastuti et al. (2019) was used in the event relocation and is listed in Table 2.

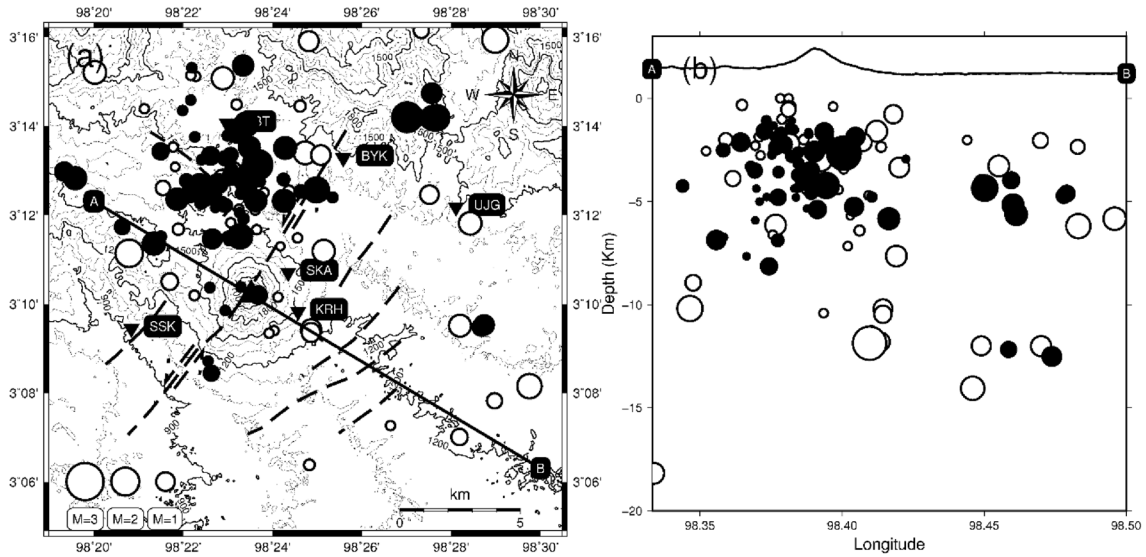


**Fig. 2** **a** Seventy-eight relocated VTs (black dots) and **b** the depth cross-section along the line AB using the GAD catalogue for the initial locations (Afnimar et al., 2020). Thirty-one un-relocated hypocentres are plotted as open circles. The dot size is graded based on the magnitude values. The other legends are the same as in Fig. 1b

**Table 1** Seismic stations used in this study

| Station | Instrument type | Location |
|---|---|---|
| UJG (ujung trans) | 3-component KSV-300, Kinkei Recording System | 03° 12′ 09.96″ N 98° 28′ 06.60″ E 1462 m |
| LBT (laubatun) | 3-component KSV-300, Kinkei Recording System | 03° 14′ 02.80″ N 98° 22′ 58.90″ E 1398 m |
| SKA (sukanalu atas) | 3-component KSV-300, Kinkei Recording System | 03° 10′ 41.8″ N 98° 24′ 20.8″ E 1610 m |
| SSK (susuk) | 3-component KSV-300, Kinkei Recording System | 03° 09′ 26.46″ N 98° 20′ 50.16″ E 914 m |
| KRH (berkerah) | 3-component KSV-300, Kinkei Recording System | 03° 09′ 49.68″ N 98° 24′ 34.14″ E 1492 m |
| BYK (kebayaken) | 3-component KSV-300, Kinkei Recording System | 03° 13′ 16.40″ N 98° 25′ 34.90″ E 1479 m |

**Table 2** The 1D velocity model used in this study for initial hypocentre determination (from Indrastuti et al., 2019). The $\alpha$ $\beta$ ratio is assumed to be 1.73

| Depth (km) | $\alpha$ (km/s) | $\rho$ (g/cm^3) |
|---|---|---|
| − 3.0 | 2.36 | 2.172 |
| − 1.0 | 2.60 | 2.220 |
| 0.0 | 2.84 | 2.268 |
| 1.0 | 3.00 | 2.300 |
| 2.0 | 3.16 | 2.332 |
| 3.0 | 3.29 | 2.358 |
| 4.0 | 3.42 | 2.384 |
| 5.0 | 3.55 | 2.410 |
| 12.0 | 4.47 | 2.594 |
| 20.0 | 5.48 | 2.800 |

## Methods

The focal mechanism inversion method developed by Kuge (1999, 2003) is applied in this research. This method uses the extended reflectivity method developed by Kohketsu (1985) to calculate the Green's function at each station from a hypocentre point. Through the inversion process, the moment tensor can be estimated. This inversion method has successfully estimated source mechanisms of, for example, the 2000 Lake Van earthquake in Turkey (Pinar et al. 2007), low-frequency earthquakes in Shikoku, Japan, (Kuge 2013), micro earthquakes along the Lembat fault (Afnimar et al. 2015). This method is good enough for limited station number as it was applied to micro events data around Lembang fault.

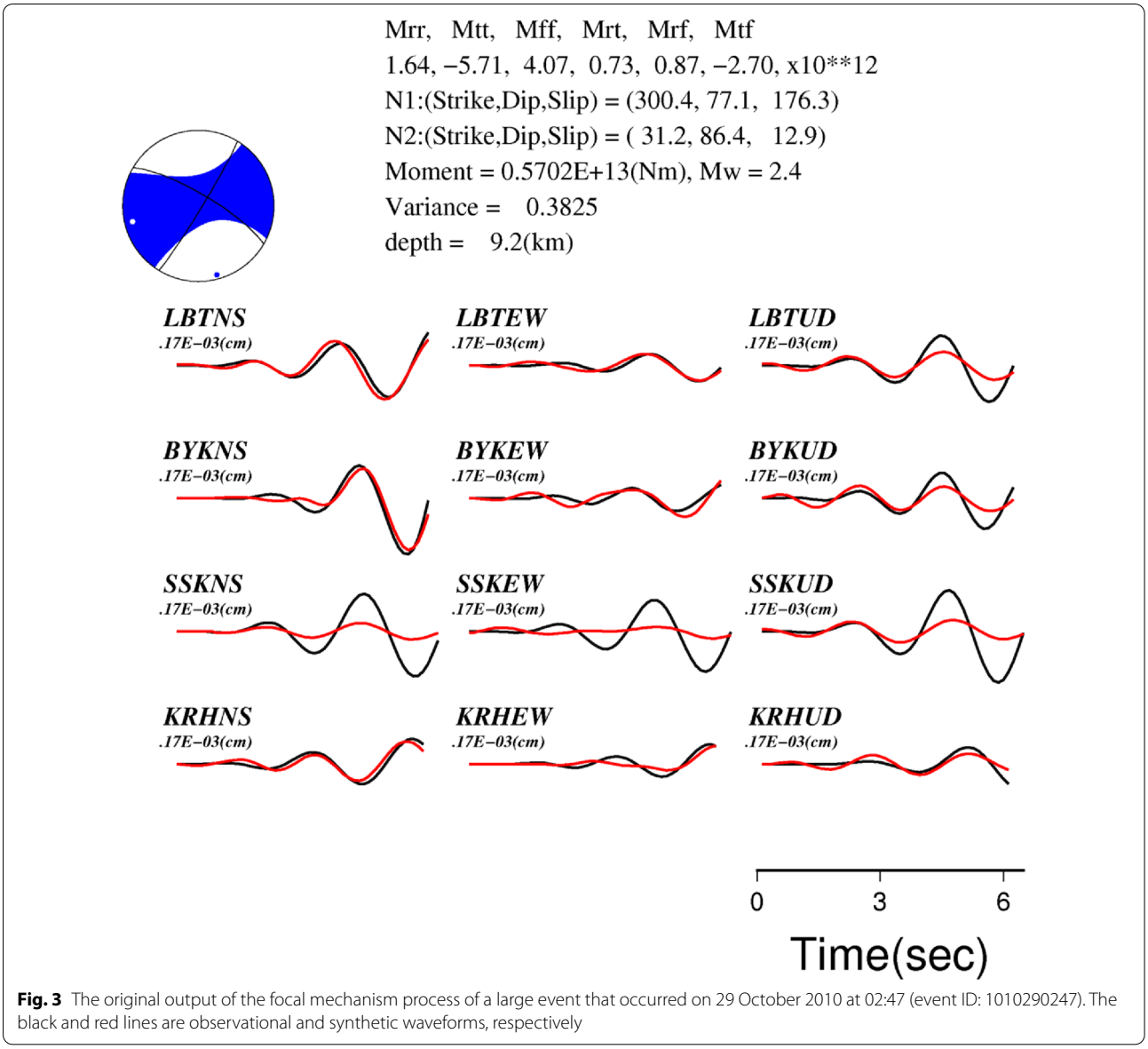


**Fig. 3** The original output of the focal mechanism process of a large event that occurred on 29 October 2010 at 02:47 (event ID: 1010290247). The black and red lines are observational and synthetic waveforms, respectively

## Result and analysis of the focal mechanism

The input of this process includes the trails of three-component waveforms from the P-wave onset to the end of the S-wave waveform. Unfortunately, each event was not recorded by all stations. Each windowed waveform is treated by removing its linear trend and mean value and followed by the tapering process. Finally, the waveform is filtered at about 0.2–1.4 Hz. All the processing procedures are conducted using SAC. The Green's function is calculated using the 1D velocity model listed in Table 2. We choose only 18 events from 109 events that can be processed because the filtered waveforms cannot show the proper waveform, such as without low frequency contents.

The original processing outputs of focal mechanism estimations for small and large events are shown in Figs. 3, 4. The waveforms from station LBT did not include in the focal mechanism estimation of the large event (Fig. 4) due to a recording problem. The fitting between observational and calculated waveforms is quite good. Both fault planes of each focal mechanism result are listed in Table 3 and plotted in Fig. 5. We divide all of the beach balls into three groups based on the mechanism similarity and geological consideration. The quantitative similarity is shown by the comparable fault parameters of the nodal plane, indicated by the bold numbers in Table 3. They are a south-east group (orange beach balls in Fig. 5) which has strike between 30° and 60°, a normal-faulting group (blue beach balls in Fig. 5) which has rake between −120° and −105° and a north-west group (red beach balls in Fig. 5) which has strike between 203° and 257°.

The first group is a south-east group (orange beach balls in Fig. 5) that is related to the sinistral-strike-slip fault line that stretches from the western boundary of Toba to the north-eastern boundary (one of the solid-dashed lines as if cut by the summit in Fig. 1b). The average parameters of this fault can be estimated from

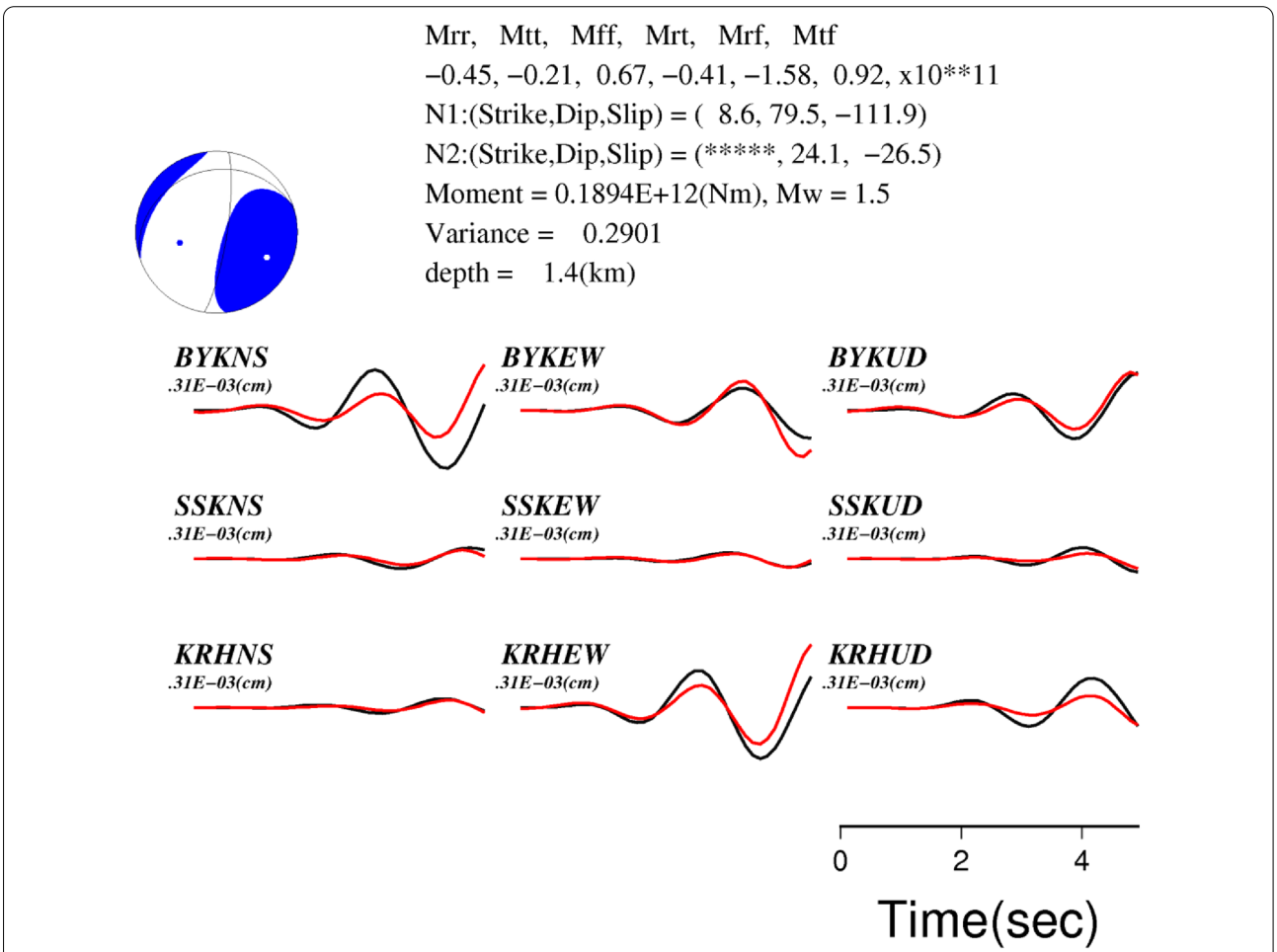


**Fig. 4** The original output of the focal mechanism process of the smallest event that occurred on 26 February 2011 at 15:24 (event ID: 1102261524). The black and red lines are observational and synthetic waveforms, respectively

**Table 3** A list of the fault plane parameters and their moment magnitude. The bold numbers are the interpreted fault planes. All these events are divided into three groups. The chosen fault plane are parameterized by bold characters

| No | Event id | N1 | | | N2 | | | Seismic moment (Nm) | Mw | Group |
|---|---|---|---|---|---|---|---|---|---|---|
| | | Strike | Dip | Rake | Strike | Dip | Rake | | | |
| 1 | 1,010,290,357 | 146.8 | 87.4 | − 158.9 | **55.9** | **68.9** | **− 2.8** | 3.29E + 12 | 2.3 | South-east group |
| 2 | 1,010,290,338 | 312.7 | 67.1 | 150.9 | **54.9** | **63.3** | **25.8** | 2.07E + 12 | 2.1 | |
| 3 | 1,010,290,247 | 300.4 | 77.1 | 176.3 | **31.2** | **86** | **12** | 5.70E + 12 | 2.4 | |
| 4 | 1,109,020,632 | 290.2 | 59.5 | 148.8 | **37.3** | **63.5** | **34.6** | 5.79E + 12 | 2.4 | |
| 5 | 1,011,280,219 | 295.5 | 62.2 | 149.7 | **40.6** | **63.5** | **31.4** | 5.38E + 11 | 1.8 | |
| 6 | 1,112,231,320 | 310.4 | 75 | 150.3 | **48.8** | **61.4** | **17.1** | 7.59E + 12 | 2.5 | |
| 7 | 1,102,261,524 | **8.6** | **79.5** | **− 111.9** | − 105.86 | 24.1 | − 26.5 | 1.89E + 11 | 1.5 | Normal-faulting group |
| 8 | 1,110,140,551 | 244.5 | 33.2 | − 27.8 | **358.3** | **75.2** | **− 120.1** | 4.13E + 12 | 2.3 | |
| 9 | 1,107,160,715 | **10.5** | **77.4** | **− 107.7** | − 113.77 | 21.6 | − 36.2 | 3.46E + 11 | 1.6 | |
| 10 | 1,112,300,522 | 63.1 | 76.4 | − 86.4 | **228** | **14.1** | **− 104.6** | 1.33E + 11 | 1.4 | |
| 11 | 1,107,160,405 | 300.9 | 76.2 | − 161 | **206.2** | **71.6** | **− 14.5** | 1.79E + 12 | 2.1 | North-west group |
| 12 | 1,110,150,200 | 322.8 | 58 | − 165.8 | **225.1** | **78** | **− 32.8** | 8.98E + 10 | 1.2 | |
| 13 | 1,110,141,709 | 307.9 | 73.4 | − 149.5 | **208.4** | **60.9** | **− 19** | 1.16E + 12 | 2 | |
| 14 | 1,107,160,040 | 352.4 | 69.1 | − 163.3 | **256.3** | **74.4** | **− 21.7** | 1.14E + 12 | 2 | |
| 15 | 1,111,200,142 | 312.5 | 43.3 | − 162.7 | **209.7** | **78.2** | **− 48.1** | 3.85E + 12 | 2.3 | |
| 16 | 1,107,160,806 | 301.6 | 83.6 | − 172.6 | **210.8** | **82.7** | **− 6.5** | 8.63E + 11 | 1.9 | |
| 17 | 1,107,161,220 | 98.2 | 57.9 | 154.4 | **202.5** | **68.5** | **34.8** | 2.24E + 11 | 1.5 | |
| 18 | 1,109,111,415 | 350.5 | 40 | − 172.4 | **254.7** | **85.2** | **− 50.3** | 1.33E + 13 | 2.7 | |

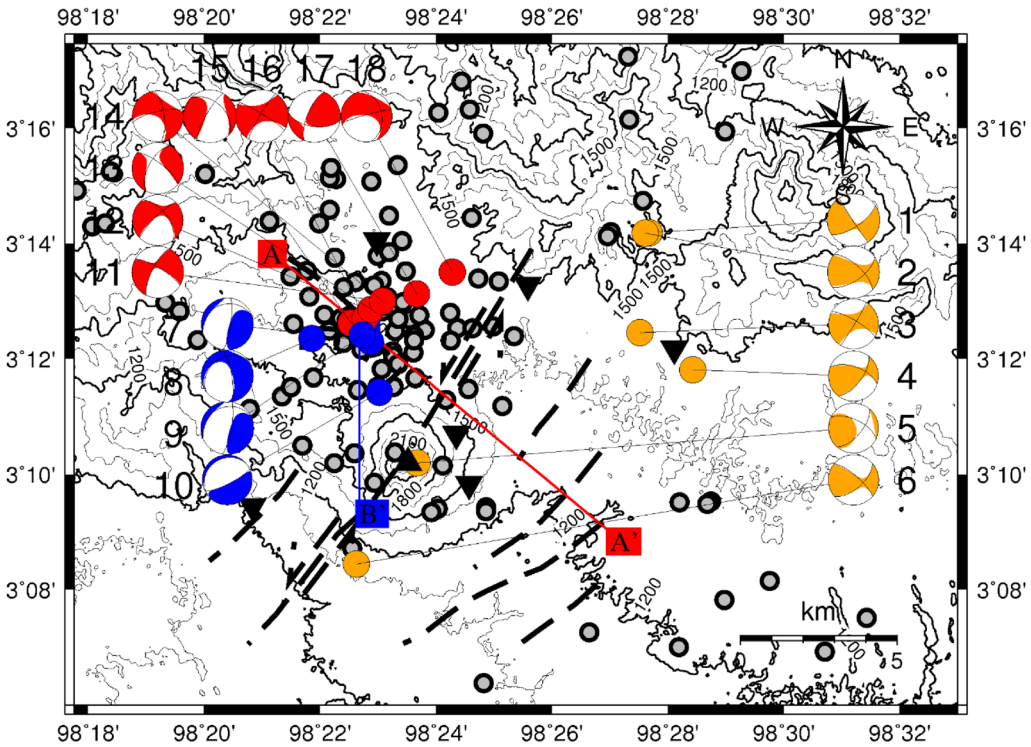


**Fig. 5** Plotting the focal mechanism results. There are three groups: the southeast group (orange beach balls), the normal-faulting group (blue beach balls), and the northwest group (red beach balls)

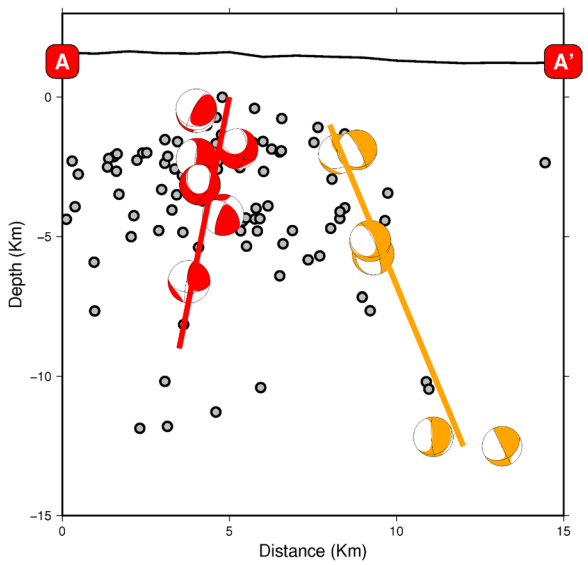


**Fig. 6** The vertical distribution of the southeast group along the AA' line in Fig. 5. The thick lines are estimated fault planes

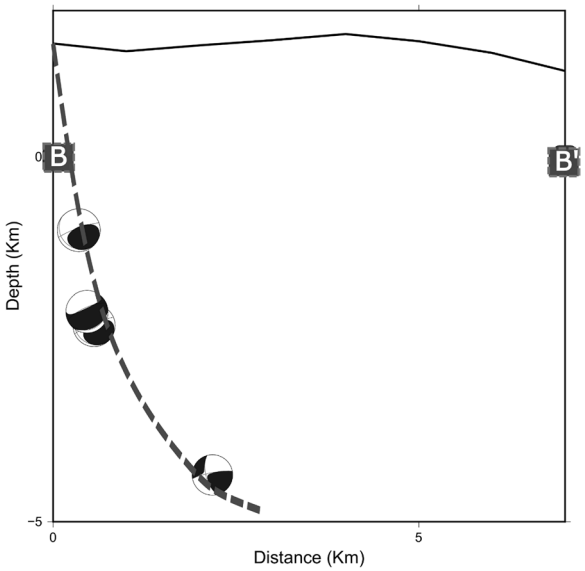


**Fig. 7** The vertical distribution of the normal-faulting group along the BB' line in Fig. 5. The dashed line is an estimated fault plane

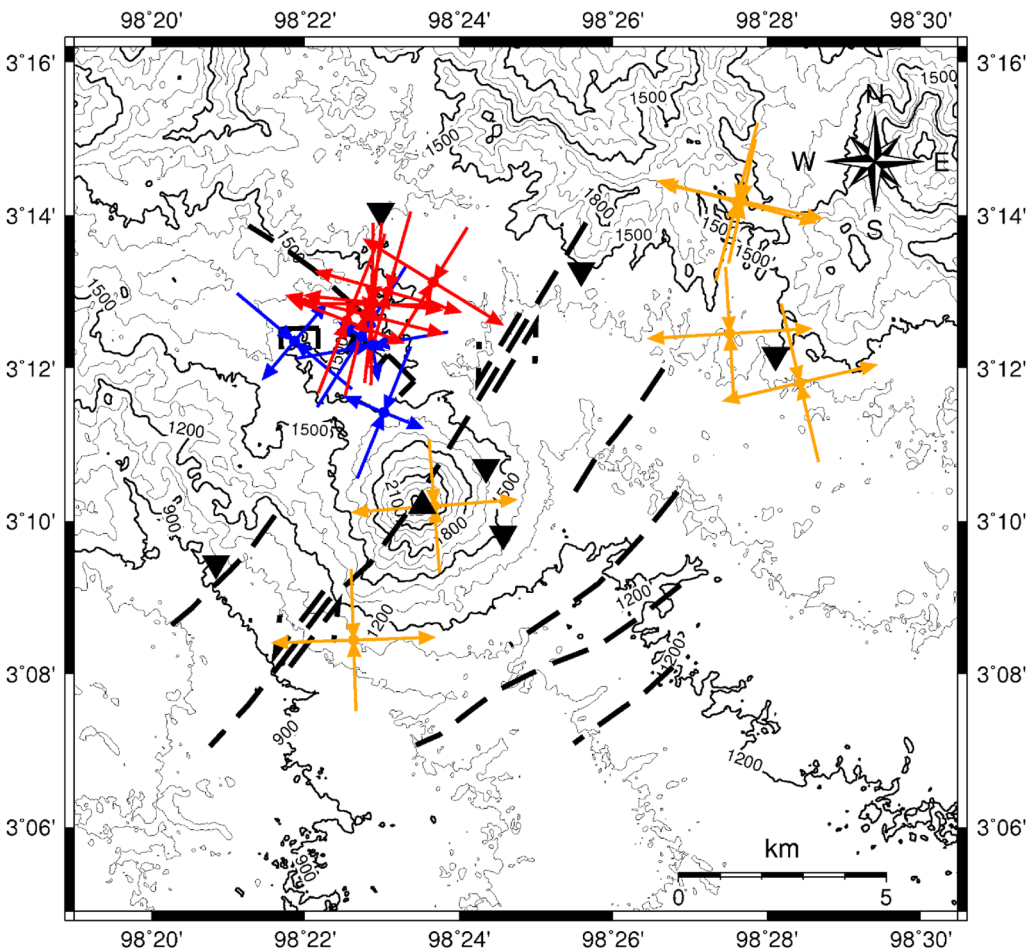


**Fig. 8** The P and T axis for all events. The color of each event is according to its group, as shown in Fig. 5

bold-character values in Table 3). They are the strike of 44.76°, the dip of 67.83° and the rake of 19.7°. This is an oblique-sinistral-strike-slip fault. The cross-section along AA' in Fig. 5, also shown in Fig. 6, emphasizes the dip of the fault. The existence of this sinistral fault has been also indicated by Prasetyo et al. 2018 from the local event with Mw 5.6. The external forces that are responsible for these events can be estimated from their pressure axes. Figure 8 shows that the most possible forces could be pressure from the south that might be related to the magma pressure induced by magma intrusion at the north-eastern parts of the study area (e.g. Hotta et al. 2018; Kriswati et al. 2018).

The second group is a normal-faulting group (the blue beach balls in Fig. 5). All of them are related to the evidence of a normal fault structure found in the northern part of the Kawar Lake area (Prambada et al. 2010). 2019. From the cross-section along the blue line in Fig. 5 that is shown in Fig. 7, the possibility of the normal fault structure can be estimated. All these normal faultings could be due to gravitational collapse. From three events except number 10 in Table 3, the strike, dip and rake are 5.8°, 77.4°, and − 113.2° of the possible fault related to the lake. We cannot interpret the geological structure related to the number 10 event.

The third group is a north-west group (the red beach balls in Fig. 5) and is a clear cluster (see their distribution in Fig. 2) that must represent a geological feature (e.g. Segall and Pollard 1980; Waldhauser and Ellsworth 2000; Santana et al. 2012). Eight events have good lineation, shown by their cross-section (Fig. 6) along the AA' line in Fig. 5. From their horizontal and vertical distributions, we can define a hidden fault in this area without topography expression. The fault parameters can be estimated from average focal parameter values as listed in bold characters in Table 3. The strike, dip and rake are 213.15°, 77.72°, and − 20.04°, respectively. This is oblique sinistral-strike-slip faulting. From their pressure axes (Fig. 8), the

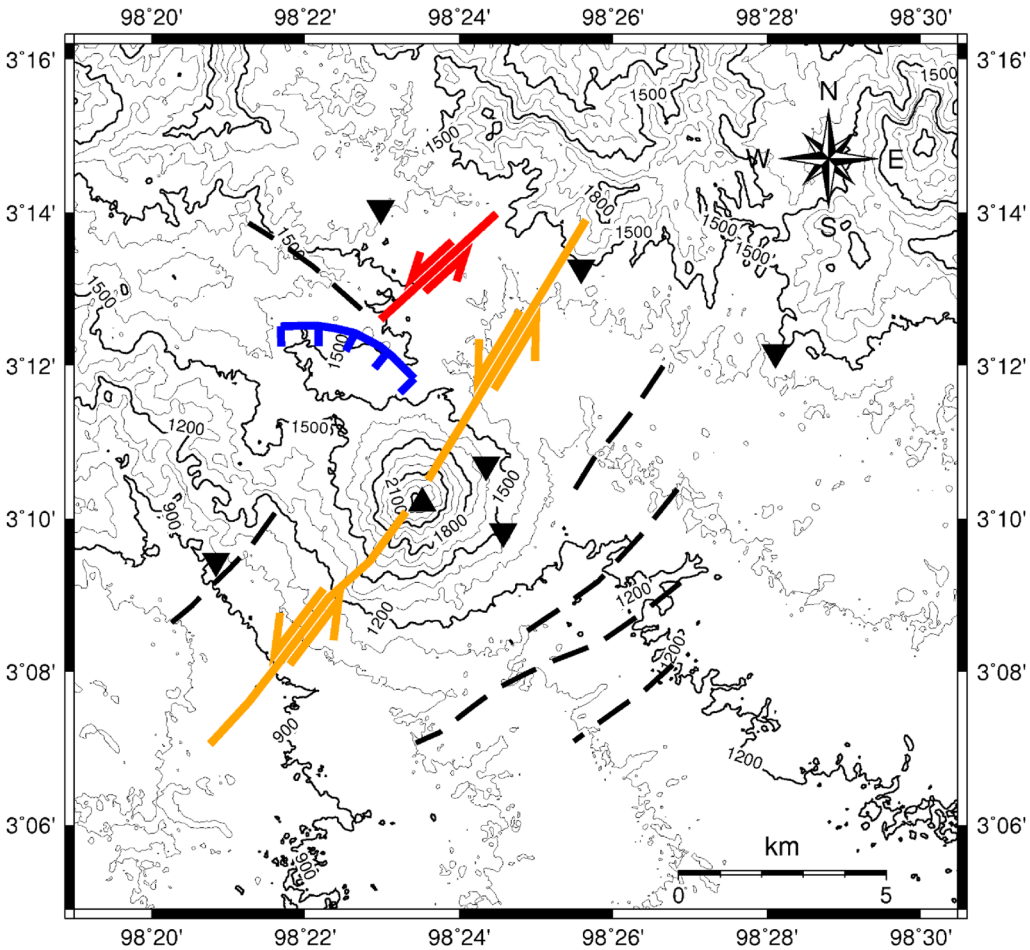


**Fig. 9** The proven fault structures from the focal mechanism results are shown by solid black, red and blue lines. The red one is a hidden fault

forces that triggered these events could be magma pressure from southern parts (e.g. Hotta et al. 2018; Kriswati et al. 2018). This result confirms the existence of a hidden fault, which corrects the previous hypothesis that this group relates to magma intrusion. All three proven faults that are analyzed above are plotted in Fig. 9.

## Conclusions

We have estimated the focal mechanisms of some dominated VT earthquakes (McCausland et al. 2019) during this research period. This research revealed one hidden fault that related to the north-west group events and confirmed two possible faults, a fault as if cut by the summit that related to the south-east group events, and a normal fault structure at Kawr Lake are that realted to the normal-faulting group events. All the events are most likely related to the activation of the fault by stress fields due to magma migration. This phenomenon has been also proven by many seismologists, e.g. Zobin 1972, Dumont et al. 2015 and White and McCausland 2016, in other volcanic areas.

**Acknowledgements**

We thank Dr. Taishi Yamada from Sakurajima Volcano Research Centre, the Disaster Prevention Research Institute, Kyoto University, an anonymous journal reviewer, and the Geoscience Letter Associate Editor for their valuable corrections of the manuscript.

**Author contributions**

AH estimated the preliminary focal mevhanisms, A improved the focal mechanism using relocated hypocenters, made all pictures and made the manuscript, K, HT, AB and NI provided the waveform data and a geological reference.

**Funding**

This research has been funded by Riset ITB 2018, by the operational funds of CVGHM, and the cooperative relationship between CVGHM and ITB.

**Availability of data and materials**

The datasets used and/or analyzed during the current study are available from the corresponding author on reasonable request.

## Declarations

**Competing interests**

The authors declare that they have no competing interests.

**Author details**

[1]Seismology and Geodynamic Laboratory, Faculty of Mining and Petroleum Engineering, Bandung Institute of Technology (ITB), Ganesha 10 Street, West Java 40132, Bandung, Indonesia. [2]Geological Agency, Centre for Volcanology and Geologic Hazard Mitigation, Jl. Diponegoro 57, Bandung 40122, Indonesia.

Received: 3 November 2020 Accepted: 1 July 2022
Published online: 12 August 2022

**References**

Afnimar E, Yulianto Rasmid E (2015) Geological and tectonic implications obtained from first seismic activity investigation around Lembang fault. Geosci Lett. https://doi.org/10.1186/s40562-015-0020-5

Afnimar MWA, Hamidah NN, Kristianto BA, Indrastuti N (2020) Local magnitude, coda magnitude, and radiated energy of volcanic tectonic earthquakes from October 2010 to December 2011 at Sinabung volcano Indonesia. Bulletin Volcanol. https://doi.org/10.1007/s00445-020-01383-7

Chouet BA, Matoza RS (2013) A multi-decadal view of seismic methods for detecting precursors of magma movement and eruption. J Volcanol Geotherm Res 252:108–175

Dumont S, Socquet A, Grandin R, Doubre KY (2015) Surface displacements on faults triggered by slow magma transfers between dyke injections in the 2005–2010 rifting episode at Dabbahu–Manda–Hararo rift (Afar, Ethiopia). Geophy J Int 204:399–417

Goldstein P, Snoke A (2005) SAC availability for the IRIS community. Incorporated Research Institutions for Seismology Newsletter 7 (UCRL-JRNL-211140)

Gunawan H, Surono BA, Kristianto PO, McCausland WA, Pallister JS, Iguchi M (2019) Overview of the eruptions of Sinabung 2010 and 2013-present and details of the phreatomagmatic phase. J Volcanol Geotherm Res 382:210–223. https://doi.org/10.1016/j.jvolgeores.2017.09.018

Hendrasto M, Surono BA, Kristianto TH, Haerani N, Basuki A, Suparman Y, Primulyana S, Prambada O, Loeqman A, Indrastuti N, Andreas AA, Rosadi U, Adi S, Iguchi M, Ohkura T, Nakada S, Yoshimoto M (2012) Evaluation of volcanic activity at Sinabung volcano, after more than 400 years of quiet. J Disaster Res 7(1):11

Hotta K, Iguchi M, Ohkura T, Gunawan H, Rosadi U, Kriswati E (2018) Magma intrusion and effusion at Sinabung volcano, Indonesia, from 2013 to 2016, as revealed by continuous GPS observation. J Volcanol Geotherm Res. https://doi.org/10.1016/j.jvolgeores.2017.12.015

Iguchi M, Ishihara K, Surono HM (2011) Learn from 2010 eruptions at Merapi and Sinabung volcanoes in Indonesia, Disaster Prev Res Inst Ann 54(B):11

Indrastuti N, Nugraha AD, McCausland WA, Hendrasto M, Gunawan H, Kusnandar R, Kasbani K (2019) 3-D seismic tomographic study of Sinabung volcano, northern Sumatra, Indonesia, during the inter-eruptive period October 2010–July 2013. J Volcanol Geotherm Res 382:197–209. https://doi.org/10.1016/j.jvolgeores.2019.03.001

Kohketsu K (1985) The extended reflectivity method for synthetic near-field seismograms. J Phys Earth 33:121–131

Kriswati E, Meilano I, Iguchi M, Abidin HZ, Surono, (2018) An evaluation of the possibility of the tectonic triggering of the Sinabung eruption. J Volcanol Geotherm Res. https://doi.org/10.1016/j.jvolgeores.2018.04.031

Kuge K (1999) Automated determination of earthquake source parameters using broadband strong-motion waveform data. EOS Trans Am Geophys Un 80:F661

Kuge K (2003) Source modeling using strong-motion waveforms: toward automated determination of earthquake fault planes and moment-release distributions. Bull Seismo Soc Am 93:639–654

Kuge K (2013) Structure down-dip of deep low-frequency earthquakes in western Shikoku, Japan, revealed by P and S waves propagating at slow apparent velocities from intraslab earthquakes. Geophys Res Lett 40:5646–5651. https://doi.org/10.1002/2013GL057781

McCausland WA, White R, Indrastuti N, Gunawan H, Patira C, Suparman Y, Putra A, Triastuty H, Hendrasto M (2019) Using a process-based model of pre-eruptive seismic patterns to forecast evolving eruptive styles at Sinabung volcano Indonesia. J Volcanol Geotherm Res 382:253–266. https://doi.org/10.1016/j.jvolgeores.2017.04.004

McNutt SR, Roman DC (2015) Volcanic seismicity In: the encyclopedia of volcanoes. academic press, pp 1011–1034

Nishi K. (2005) Hypocenter calculation software GAD (Geiger's method with adaptive damping) GAD manual guide

Pinar A, Honkura Y, Kuge K, Matsushima M, Sezgin N, Yilmazer M, Öğütçü Z (2007) Source mechanism of the 2000 November 15 Lake Van earthquake (Mw = 5.6) in eastern Turkey and its seismotectonic implications. Geophys J Int 170:749–763. https://doi.org/10.1111/j.1365-246X.2007.03445

Prambada O, Zaennudin A, Iryanto, Basuki A, Yulius C, Mulyadi, Rohaeti E, Kisroh, Suparmo (2010) Report of geological mapping of Sinabung volcano, regency of Karo, province of north Sumatera center for volcanology and geological hazard Mitigation unpublished report (in Indonesian)

Prasetyo RA, Heryandoko N, Sianipar DSJ, Suardi I, Rohadi S (2018) The source mechanism analysis of significant local earthquake Mw 5.6 January 16, 2017 near Mt. Sibayak and Mt. Sinabung using moment tensor inversion of BMKG waveform data, AIP Conference proceedings, (1987), 020078

Roman DC, Cashman KV (2006) The origin of volcano-tectonic earthquake swarms. Geology 34(6):457–460
Santana FL, Medeiros WE, do Nascimento AF, Bezerra FHR (2012) Hypocentral relocation using clustering-along-palnes constraints: implications for fault geometry. Geophys J Int 190:1077–1090
Segall P, Pollard DD (1980) Mechanics of discontinuous fault. J Geophys Res 85:4337–4350
Sieh K, Natawidjaja D (2000) Neotectonics of the Sumatran fault Indonesia. J Geophys Res 105(B12):28295. https://doi.org/10.1029/2000JB900120
Waldhauser W, Ellsworth WL (2000) A double-difference earthquake location algorithm: method and application to the northern hayward fault California. Bull Seismol Soc Am 90:1353–1368
Walter TR, Amelung F (2007) Volcanic eruptions following M ≥ 9 megathrust earthquakes: implications for the Sumatra-Andaman volcanoes. Geology 35:539–542
White R, McCausland W (2016) Volcano-tectonic earthquakes: a new tool for estimating intrusive volumes and forecasting eruptions. J Volcanol Geotherm Res 309:139–155
White RA, McCausland WA (2019) A process-based model of pre-eruption seismicity patterns and its use for eruption forecasting at dormant stratovolcanoes. J Volcanol Geotherm Res 382:267–297. https://doi.org/10.1016/j.jvolgeores.2019.03.004
Zoback ML, Geist E, Pallister J, Hill DP, Young S, McCausland WA (2013) Advances in natural hazard science and assessment, 1963–2013. Geol Soc Am Spec Pap 501:81–154
Zobin VM (1972) Focal mechanism of volcanic earthquakes. Bulletin Volcanologique 36:561–571

## Publisher's Note